Physiological Characterization of a Plant Mitochondrial Calcium Uniporter in Vitro and in Vivo[1]

Enrico Teardo*, Luca Carraretto, Stephan Wagner, Elide Formentin, Smrutisanjita Behera, Sara De Bortoli, Véronique Larosa, Philippe Fuchs, Fiorella Lo Schiavo, Anna Raffaello, Rosario Rizzuto, Alex Costa, Markus Schwarzländer, and Ildiko Szabò*

Department of Biology (E.T., L.C., E.F., S.D.B., V.L., F.L.S., I.S.) and Department of Biomedical Sciences (A.R., R.R.), University of Padova, 35121 Padova, Italy; CNR Institute of Neuroscience, Padova, Italy, Department of Biomedical Sciences, University of Padua, 35121 Padova, Italy (E.T., I.S.); Plant Energy Biology Lab, Institute of Crop Science and Resource Conservation (INRES), University of Bonn, 53113 Bonn, Germany (S.W., P.F., M.S.); Department of Biosciences, University of Milan, 20133 Milan, Italy (S.B., A.C.); and Institute of Biophysics, Consiglio Nazionale delle Ricerche, 20133 Milan, Italy (A.C.)

ORCID IDs: 0000-0001-5369-7911 (S.W); 0000-0001-8749-6130 (S.B.); 0000-0003-3797-6966 (S.D.B.); 0000-0001-6379-853X (P.F.); 0000-0002-2628-1176 (A.C.); 0000-0003-0796-8308 (M.S.); 0000-0002-3637-3947 (I.S.).

Over the recent years, several proteins that make up the mitochondrial calcium uniporter complex (MCUC) mediating Ca^{2+} uptake into the mitochondrial matrix have been identified in mammals, including the channel-forming protein MCU. Although six *MCU* gene homologs are conserved in the model plant Arabidopsis (*Arabidopsis thaliana*) in which mitochondria can accumulate Ca^{2+}, a functional characterization of plant MCU homologs has been lacking. Using electrophysiology, we show that one isoform, AtMCU1, gives rise to a Ca^{2+}-permeable channel activity that can be observed even in the absence of accessory proteins implicated in the formation of the active mammalian channel. Furthermore, we provide direct evidence that AtMCU1 activity is sensitive to the mitochondrial calcium uniporter inhibitors Ruthenium Red and Gd^{3+}, as well as to the Arabidopsis protein MICU, a regulatory MCUC component. AtMCU1 is prevalently expressed in roots, localizes to mitochondria, and its absence causes mild changes in Ca^{2+} dynamics as assessed by in vivo measurements in Arabidopsis root tips. Plants either lacking or overexpressing AtMCU1 display root mitochondria with altered ultrastructure and show shorter primary roots under restrictive growth conditions. In summary, our work adds evolutionary depth to the investigation of mitochondrial Ca^{2+} transport, indicates that AtMCU1, together with MICU as a regulator, represents a functional configuration of the plant mitochondrial Ca^{2+} uptake complex with differences to the mammalian MCUC, and identifies a new player of the intracellular Ca^{2+} regulation network in plants.

Plants respond to changes in their environment by adjusting their metabolism and physiology. The ability of plants to react with high specificity to a given stimulus is of vital importance. Among the different signal transduction mechanisms, Ca^{2+} plays a prominent role as a second messenger (Love et al., 2004; McAinsh and Pittman, 2009; Dodd et al., 2010). In animal cells, transient accumulation of Ca^{2+} in intracellular organelles shapes cytosolic Ca^{2+} transients (e.g. Rizzuto et al., 2012), and a similar concept has been suggested for plants (Nomura and Shiina, 2014).

Free Ca^{2+} concentrations in the cytosol are maintained at much lower (~10,000-fold less) levels than in the extra-cellular space. Steep electrochemical gradients across the plasma and intracellular membranes allow the generation of time-resolved Ca^{2+} transients in response to external stimuli and as part of developmental processes (e.g. pollen and root hair elongation). Beside the endoplasmic reticulum that functions as intracellular Ca^{2+} store in animal cells, plant cells contain additional intracellular stores such as the vacuole and the chloroplast thylakoid lumen (e.g. Stael et al., 2012).

In animal cells, mitochondrial Ca^{2+} uptake and release have a fundamental regulatory role in various physiological processes, ranging from controlling insulin secretion to cell death and muscle contraction (De Stefani et al., 2015). Mitochondrial Ca^{2+} uptake has been extensively studied, but the molecular identity of the involved proteins has been elucidated only recently. Five years ago, the Mootha group and some of us independently identified a 40-kD protein (Mitochondrial Calcium Uniporter [MCU]) that gives rise to Ca^{2+}-permeable channel activity. The MCU was proposed to be the core component of the calcium uniporter of the inner mitochondrial membrane (Baughman et al., 2011; De Stefani et al., 2011). MCU showed channel activity in planar lipid bilayers (De Stefani et al., 2011) with electrophysiological properties and inhibitor sensitivity of the uniporter (to Ruthenium Red [RR] and Gd^{3+}), previously identified as a Ca^{2+}-permeable ion channel in patch clamp experiments on mammalian mitoplasts (Kirichok et al., 2004). Furthermore, siRNA against the MCU protein abolished the mitochondrial Ca^{2+} current recorded in mitoplasts (Chaudhuri et al., 2013). MCU does not share amino acid sequence similarity with known Ca^{2+} channels in plants

or animals, but its pore region contains several negatively charged amino acids that are crucial for Ca^{2+} transport (De Stefani et al., 2011). In this region, a highly conserved Ser residue is involved in binding of the inhibitor RR (Baughman et al., 2011). The consensus view concerning topology of MCU is that both N- and C-terminal domains face the mitochondrial matrix, with the two membrane-spanning domains connected in the intermembrane space by a short pore loop. The structure of the N-terminal domain has been resolved first, revealing that the N-terminal domain preceding the first coiled domain is essential for the modulation of MCU function: overexpression of MCU lacking this domain had a dominant-negative effect on mitochondrial Ca^{2+} uptake (Lee et al., 2015). A more recent structural study suggests that similarly to some other classical ion channels, pentamerization of the two transmembrane-helix containing subunits is required for formation of a functional channel (Oxenoid et al., 2016, see also "Discussion"). Both primary sequence and the predicted three-dimensional structure indicate that the MCU protein forms channels with distinct features from Ca^{2+}-carrying Na^+/Ca^{2+} and H^+/Ca^{2+} exchangers.

Following the discovery and initial characterization of MCU and the EF-hand containing regulator Mitochondrial Calcium Uptake 1 (MICU1; Perocchi et al., 2010), which also has a muscle-specific alternative splice isoform with higher Ca^{2+} binding affinity than MICU1 (Vecellio Reane et al., 2016), several additional proteins forming the mammalian MCU complex (MCUC) have been identified. These proteins include Essential MCU Regulator (EMRE; Sancak et al., 2013), MCU Regulator 1 (MCUR1; Mallilankaraman et al., 2012), and MCUb (a dominant negative MCU isoform; Raffaello et al., 2013) as well as MICU2 and 3 (Plovanich et al., 2013; Patron et al., 2014). All these components were reported to be essential components and/or regulators of MCUC (for recent reviews see, e.g. De Stefani et al., 2015; Foskett and Philipson 2015).

Ca^{2+} uptake has been studied in isolated plant mitochondria for over half a century, providing comprehensive evidence for the presence of a functional transport system (Hanson et al., 1965; Zottini and Zannoni, 1993; Dieter and Marmé, 1980). However, several contrasting results remain unresolved, and even the existence of a RR-sensitive, uniporter-like transport mechanism has been questioned (see e.g. Carnieri et al., 1987 versus Akerman and Moore, 1983). Aequorin-based measurements of free Ca^{2+} in the cytosol and the mitochondrial matrix of intact Arabidopsis (*Arabidopsis thaliana*) seedlings revealed slightly higher baseline Ca^{2+}, slower onset, lower amplitude, and longer recovery times for mitochondrial matrix transients triggered by environmental stimuli as compared to their cytosolic counterparts (Logan and Knight, 2003). This general pattern was confirmed using Yellow Cameleon sensors (Loro et al., 2012; Wagner et al., 2015). A molecular basis of the regulation of Ca^{2+} import into plant mitochondria and the formal demonstration of the existence of an RR-sensitive pathway has been lacking, however (Wagner et al., 2016).

Plants possess homologs of the mammalian uniporter components MCUR1, MICU, and MCU (Wagner et al., 2016). We recently provided evidence that the only MICU homolog in Arabidopsis regulates mitochondrial Ca^{2+} dynamics in intact plants (Wagner et al., 2015), but the identity of the channel remained speculative and direct evidence for regulation of a channel formed by plant MCU homologs has been missing. In the Arabidopsis genome, six genes are present that can be identified as putative MCU channel proteins, since they are homologs of human MCU counterparts sharing the transmembrane domains, the pore-loop domain, and the conserved DVME (Asp-Val-Met-Glu) signature sequence (Stael et al., 2012). On the other hand, the overall sequence similarity is relatively low; thus, functional properties cannot be straightforwardly inferred from data on mammalian MCU. Various bioinformatic tools (e.g. ChloroP, TargetP, see also Aramemnon database) predict five of the six Arabidopsis MCU isoforms to localize to the mitochondria (Schwacke et al., 2003; Carraretto et al., 2016). MCUR1 has been controversially discussed as a cytochrome *c* oxidase assembly factor instead of being an MCUC component in animals (Paupe et al., 2015; Vais et al., 2015) and, interestingly, one of the two homologs of MCUR1 in Arabidopsis has been described independently over a decade

[1] This work was supported by the Italian Ministry (PRIN grant 2010CSJX4F_005), the University of Padova (Progetto di Ateneo), and the Human Frontiers Science Program (HFSP RPG0052) to I.S. An EMBO short-term fellowship was awarded to E.T. A.C. acknowledges funding by Ministero dell'Istruzione, dell'Università e della Ricerca through the FIRB 2010 program (RBFR10S1LJ_001). M.S. thanks the Deutsche Forschungsgemeinschaft for funding through the Emmy-Noether program (SCHW1719/1-1), the Research Training Group GRK2064, and a grant (SCHW1719/5-1) as part of the package PAK918. V.L. is a Chargé de Recherche of the Belgian FNRS in mobility at Padova University thanks to a Marie-Curie fellowship (Piscopia).

* Address correspondence to ildi@civ.bio.unipd.it or enrico.teardo@unipd.it.

The authors responsible for distribution of materials integral to the findings presented in this article in accordance with the policy described in the Instructions for Authors (www.plantphysiol.org) are: Enrico Teardo (enrico.teardo@unipd.it) and Ildiko Szabò (ildi@civ.bio.unipd.it).

E.T. designed and performed the research (electrophysiology, genotyping, generation of GFP-fusion constructs, and overexpressing lines), analyzed the data, and cowrote the article; L.C. performed the confocal microscopy and TEM analysis and assayed root growth; S.W. analyzed time-lapse imaging, performed phylogenetic analysis, and measured respiratory parameters in isolated mitochondria together with P.F.; S.D.B. purified MICU, assessed photosynthetic efficiency, and performed genotyping; E.F. carried out gene expression and confocal image analysis; S.B. performed Ca^{2+} measurements; V.L. performed BN-PAGE; F.L.S. discussed data and contributed to genetic analysis; R.R. and A.R. contributed data analysis and interpretation; A.C. designed and performed time-lapse imaging and assisted in writing the manuscript; M.S. supervised the research and assisted in writing the manuscript; I.S. conceived, performed, and supervised the research and wrote the article.

www.plantphysiol.org/cgi/doi/10.1104/pp.16.01359

ago as Cox X6, a plant-specific subunit of complex IV (Millar et al., 2004; Klodmann et al., 2011). Altogether, the plant homologs of MCU and MICU1 represent good candidates for an involvement in mitochondrial Ca^{2+} homeostasis, regulation, and signaling.

In this study, we explore the functional properties of an MCU in plants. We show that MCU1 from Arabidopsis (AtMCU1) forms a functional Ca^{2+}-permeable channel that can be regulated by the Arabidopsis MICU protein. Based on our characterization at single channel level, we identify conserved and distinct characteristics in composition and function of the MCUC in mammals and Arabidopsis. To gain further insight into the physiological role of AtMCU1 in the plant, we assess Arabidopsis lines lacking or overexpressing AtMCU1.

RESULTS

Phylogenetic Analysis of MCU Homologs in the Plant Kingdoms

A recent phylogenetic analysis of MCU across the eukaryotic domain revealed that homologs of MCU are distributed widely across all major branches of eukaryotic life, present in plants and metazoa, but with apparent loss in certain protozoan and fungal lineages (Bick et al., 2012; Stael et al., 2012; Meng et al., 2015). We performed a refined phylogenetic analysis focusing on 36 species from the plant kingdom (Fig. 1A; Supplemental Fig. S1). This highlights that most species harbor three or more MCU homologs, except green algae (*Chlamydomonas reinhardtii*) and *Volvox carteri*, with only one homolog each. The DIME motif found in the pore region of mammalian MCUs is altered to DVM(E/D) in almost all plant species examined (Fig. 1B; Supplemental Fig. S1). Exceptions occur for *Physcomitrella patens* and *Brachypodium distachyon* where the D in individual isoforms is replaced by N and S, respectively. Among the six isoforms of Arabidopsis, At1g09575 (AtMCU1) and At1g57610 (AtMCU2) group together, while the other four isoforms (AtMCU3-6) belong to a more distant group. Our phylogenetic analysis did not identify any homolog of MCUb in plants. MCUb carries two conserved exchanges in R and E residues (marked in blue and red, respectively, in Supplemental Fig. S1) close to the pore loop and was suggested to form mixed oligomers with MCU resulting in a channel that does not permit the passage of Ca^{2+} (Raffaello et al., 2013), acting as dominant negative subunit. Among the different species, only *C. reinhardtii* harbors an MCU variant in which the positively charged Arg is replaced by a Tyr.

Arabidopsis MCU Homolog AtMCU1 Forms an Ion Channel

Among the six Arabidopsis isoforms, *At1g09575* is globally expressed across plant tissues and developmental stages according to the Genvestigator database (Zimmermann et al., 2004). Its amino acid sequence

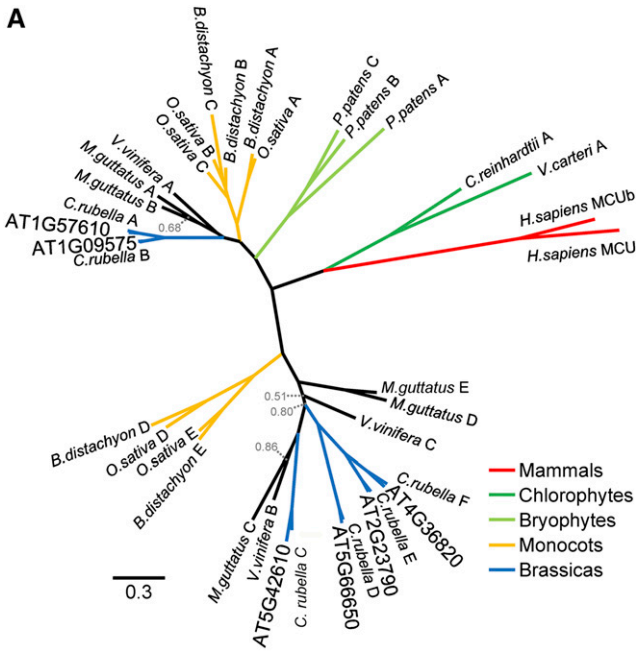

B

AT1G09575	AtMCU1	FFRLTFWEFSWDVMEPI
AT1G57610	AtMCU2	FVRLTFWEFSWDVMEPI
AT2G23790	AtMCU3	FMRLTFWELSWDVMEPI
AT4G36820	AtMCU4	FMRLTFWDLTWDVMEPI
AT5G42610	AtMCU5	FMRLTFWELSWDVMEPI
AT5G66650	AtMCU6	FFRLTFWELSWDVMEPI
H.sapiens	MCU	LARLTWWEYSWDIMEPV
H.sapiens	MCUb	LAWLTWWVYSWDIMEPV

Figure 1. Evolutionary conservation of the mitochondrial calcium uniporter in the plant kingdom. A, A phylogenetic tree of proteins from selected plant species with homology to human MCU and MCUb. Arabidopsis proteins are represented with their TAIR identifier. Scale bar corresponds to a distance of 30 changes per 100 amino acid positions. The tree robustness is expressed in posterior probabilities that are shown for nodes with values below 0.9. B, Alignment of Arabidopsis and human MCU orthologs showing the intermembrane space-facing loop between the transmembrane domains. The DIME motif (purple) is essential for Ca^{2+} transport. Additionally, mammalian MCUb that carries two conserved exchanges in nearby Arg (blue) and Glu (red) residues was shown to be able to form a multimeric ion channel that does not allow passage of Ca^{2+}.

shows homology to the mammalian MCU (36.8% identity and 71.9% similarity in a 114-amino acid overlap corresponding to amino acid 215–328 of human MCU). Mammalian MCU has a predicted N-terminal targeting sequence of 50 amino acids (Supplemental Table S1). Yet an experimental assessment of the import mechanism and the cleavage site is pending. Since AtMCU1 (*At1g09575*) has the highest mitochondrial targeting score (Stael et al., 2012; Supplemental Table S1), we focused our further analyses on this isoform. Since Arabidopsis mitoplasts (mitochondria without outer membrane) are not suitable to patch clamp because of their small size, the protein was expressed in an in vitro system (Fig. 2A). This system avoids contamination by other, and often more abundant, membrane

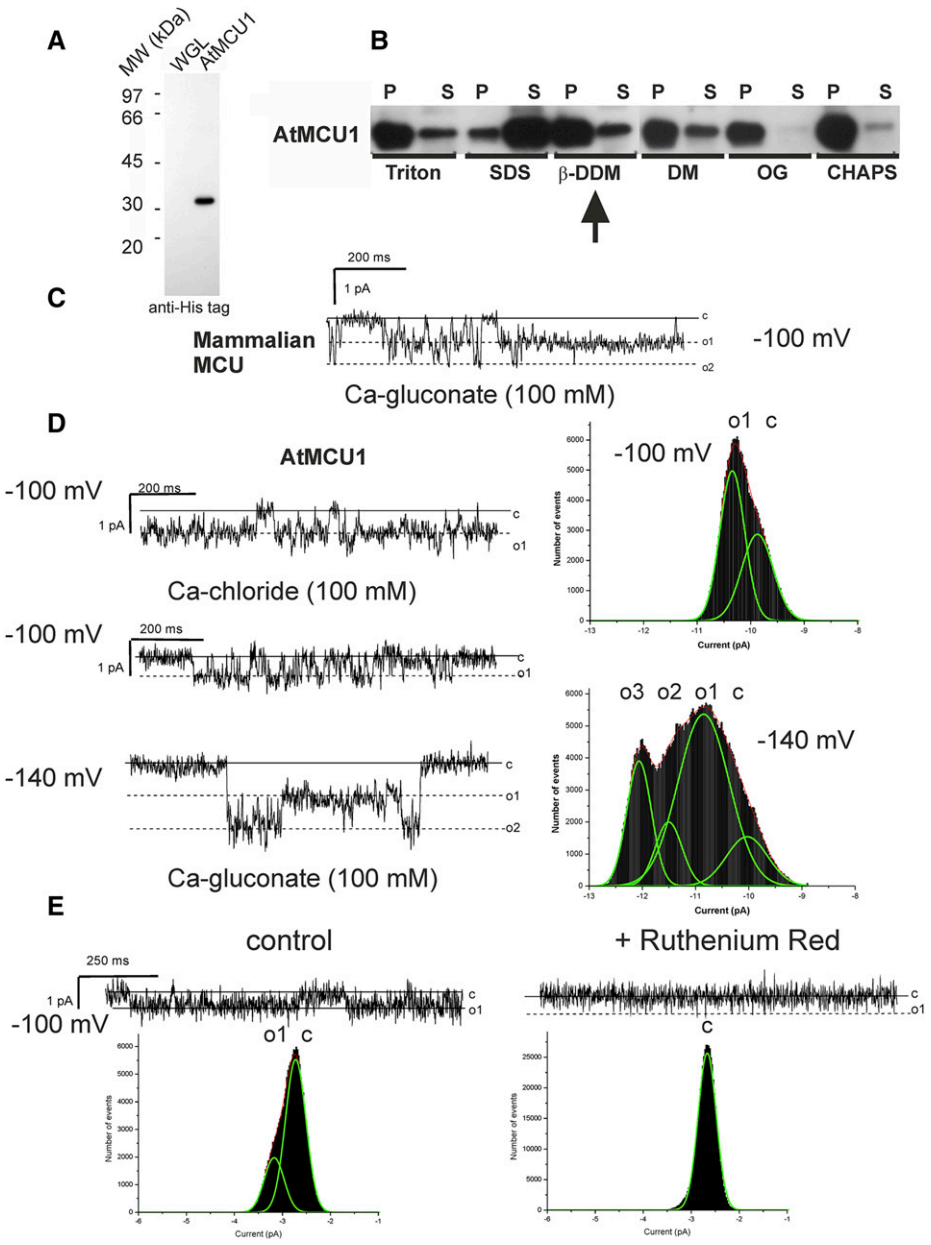

Figure 2. AtMCU1 forms a Ca^{2+}-permeable channel. A, AtMCU1 was expressed in vitro using a Wheat Germ Lysate Kit. Empty reaction mix (WGL) and mix following expression of the protein (AtMCU1) were separated by SDS-PAGE and assayed with anti-His tag antibody. B, Solubilization of in vitro-expressed AtMCU1 with 2% (w/v) of each detergent. SDS was used as a positive control. Following centrifugation, pellets (P) and supernatants (S) were separated by SDS-PAGE; anti-His tag antibody was used to detect AtMCU1. Nondenaturant β-DDM was selected for protein treatment. C, Representative current trace recorded in planar lipid bilayer at −100 mV (cis side) in the indicated solutions using recombinant mammalian MCU (obtained as described in Raffaello et al., 2013). D, Representative current traces recorded in planar lipid bilayer using AtMCU1, at the indicated voltages (cis side) in the indicated solutions. Closed (c) and open (o) states are indicated. Right, amplitude histograms obtained from 60-s traces from another experiment in 100 mM Ca-gluconate, illustrating that the channel is more active at increasing negative voltage, similarly to mammalian MCU. E, Current recorded from another experiment in 100 mM Ca-gluconate solution in the absence (control) and presence of 10 μM RR, respectively. RR, a classical inhibitor of mitochondrial Ca^{2+} uniport activity, completely abolished channel activity (see respective amplitude histograms below). Similar activity under the same conditions was observed in 11 additional independent experiments, and inhibition by RR and Gd^{3+} (Supplemental Fig. S2B) was assessed four times each.

proteins that might also be able to form channels and has been instrumental in several recent studies (e.g. C.J. Braun et al., 2014; Deniaud et al., 2010; Herdean et al., 2016). To optimize protein solubilization conditions, six different detergents were empirically tested. Dodecylmaltoside (β-DDM) proved to be the most suitable detergent and was favored over SDS due to its weak-denaturing properties (Fig. 2B).

Next, the electrophysiological characteristics of the in vitro-expressed protein were studied in a planar lipid bilayer system. Because of the low conductance of the channel, physiological concentration of Ca^{2+} (in the sub-μM range) could not be used to reveal single channel characteristics, which is similar to studies with mammalian MCU. Thus, we performed electrophysiological experiments in a medium containing 100 mM Ca^{2+} as the only cation (see also e.g. Kirichok et al., 2004). When using recombinant mammalian MCU, we observed the characteristic MCU activity (Fig. 2C). Under the same conditions, using AtMCU1, a current carried by Ca^{2+} was observed with a channel activity of very small conductance (5.4 ± 0.6 pS; mean ± SD; $n = 11$; Fig. 2, D and E) as determined from the current-voltage relationship (Supplemental Fig. S2A). The conductance and kinetic behavior resemble those observed with the mammalian MCU recorded under the same condition (Fig. 2C; Raffaello et al., 2013). Activity was observed with the same characteristics in $CaCl_2$ (Fig. 2D, upper current trace) and in Ca-gluconate (Fig. 2D, lower two traces),

indicating that the ionic current was carried by Ca^{2+}. The channel was more active at increasing, highly negative potentials as illustrated by the current traces recorded in an experiment at various applied transmembrane potentials (Fig. 2D, bottom) and amplitude histograms from another experiment (Fig. 2D, right). The channel was selective for Ca^{2+} over Cl^- displaying a permeability ratio of P_{Cl}:P_{Ca} = 0.1 ± 0.07:1.0 (± indicates SD, n = 3), as determined from the reversal potential under asymmetric ionic conditions (300 mM/100 mM $CaCl_2$; Supplemental Fig. S2A) and calculated according to the Goldman-Hodgkin-Katz equation (Hille, 1978). Importantly, and in accordance with the presence of a conserved Ser residue in the pore loop (Baughman et al., 2011), channel activity was blocked by RR, a well-characterized inhibitor of the mitochondrial calcium uniporter (Fig. 2E).

When AtMCU1 currents were recorded in a Na-gluconate low-divalent ion solution (10 pM calculated free Ca^{2+}, 100 mM Na-gluconate), RR- and Gd^{3+}-sensitive channel activity with a conductance of 57 ± 12 pS was observed (n = 35; Fig. 3A; Supplemental Fig. S2B). This is in accordance with the recognized characteristic of Ca^{2+} channels, including mammalian MCU, to allow the passage of Na^+ upon removal of Ca^{2+} and divalent cations (e.g. Hess and Tsien, 1984; Lepple-Wienhues and Cahalan, 1996; Talavera and Nilius, 2006). As in the case of the mammalian MCU, the conductance of the channel, as determined from the I-V curve, was significantly higher in the low-divalent solution than in the presence of 100 mM Ca^{2+}. While those

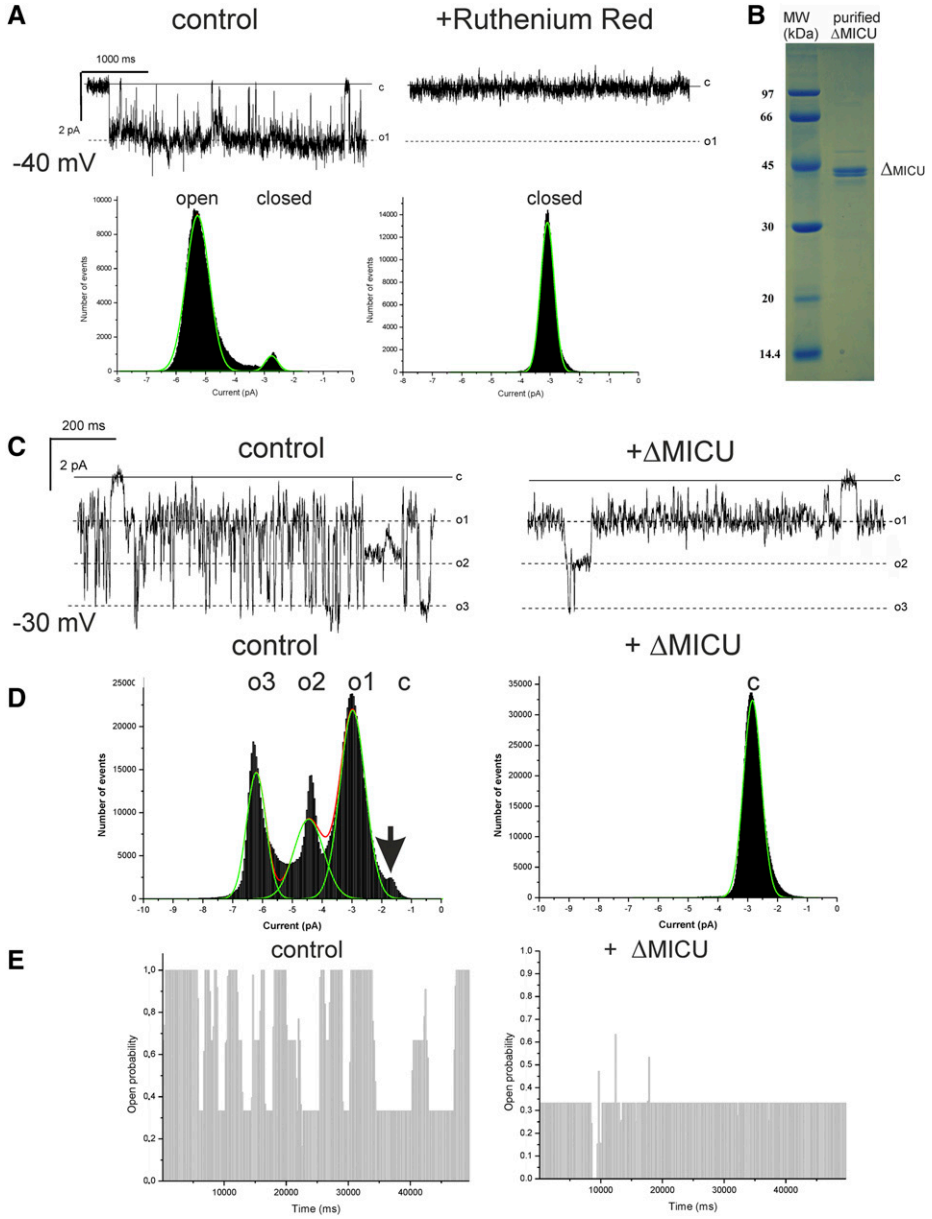

Figure 3. The impact of Arabidopsis ΔMICU on AtMCU1 channel activity. A, AtMCU1 activity recorded in the low-divalent cation medium (100 mM Na-gluconate) before (control) and after addition of 10 μM RR (V_{cis} = −40 mV; n = 4). Similar activity was observed in 22 additional independent experiments. Bottom, related amplitude histograms. B, SDS-PAGE showing purity of recombinant Arabidopsis ΔMICU purified by affinity chromatography and used in electrophysiological experiments. C, Purified ΔMICU protein was added to AtMCU1 in bilayer experiments using low-divalent solution. V_{cis} = −30 mV. D, Amplitude histograms before (control) and after addition of purified ΔMICU (0.7 ng/mL). An arrow on the histogram indicates the closed state. E, P_o density histograms for open channel level. P_o as a function of time was monitored and measured for the indicated times from the same experiment of C. The P_o was calculated for each time segment (automatically binned by PSTAT) as the mean integral current divided by the maximum current that could be attained if the channels present in the membrane were continuously open (P_o = 1). Analysis was performed using the Fetchan and PSTAT programs of PCLAMP8.0 software. The mean P_o decreased from 0.67 to 0.32 in this representative experiment; a decrease to similar extent was observed in five additional independent experiments.

specific electrophysiological characteristics make a strong case for functional conservation, it needs emphasizing that this observation does not mean that the channel is mediating Na^+ flux under physiological conditions, since the concentrations of divalent cations exceeds 10 pM, and this results in a block of the Na^+ current (Kirichok et al., 2004; Raffaello et al., 2013). The electrophysiological observations strongly indicate that AtMCU1 can give rise to a functional, Ca^{2+}-permeable channel with comparable characteristics to those observed for the mammalian MCU and compatible with an RR-sensitive uniporter function.

Arabidopsis MICU Inhibits AtMCU1 Activity

We next assessed whether and how the only Arabidopsis homolog of the mammalian MICU family impacts AtMCU1 function. Addition of purified Arabidopsis ΔMICU (Fig. 3B) drastically and reproducibly reduced the channel activity of AtMCU1 ($n = 6$) at low Ca^{2+} concentrations (low-divalent solution, see above; Fig. 3, C–E). ΔMICU lacks the first 117 amino acids comprising the signal peptide and putative transmembrane/disordered sequences, which are cleaved off in the mammalian isoform (Petrungaro et al., 2015), and carries an N-terminal His-tag. All predicted EF hand motifs remain intact, and we have previously found that ΔMICU can bind Ca^{2+} (Wagner et al., 2015). In the low-divalent solution ΔMICU, which has been suggested to exert a gatekeeping function in plants under resting conditions, is unlikely to bind any Ca^{2+} (Wagner et al., 2015). In a representative experiment (Fig. 3C), three channels were present displaying high open probability (mean P_o , 0.67). Following addition of ΔMICU, only one channel remained partially open and the overall P_o significantly decreased (to mean P_o of 0.32) as observable from the respective amplitude histograms (Fig. 3D). These observations, which were confirmed in five additional independent experiments leading to a drastic decrease of the mean P_o (Fig. 2E), indicate that the presence of MICU inhibits the channel activity of AtMCU1 at low free Ca^{2+} levels, similarly to mammalian MICU2 (Patron et al., 2014). They further validate previous findings in vivo, where absence of MICU in Arabidopsis led to elevated resting concentrations of free matrix Ca^{2+} in unstimulated root tissue (Wagner et al., 2015).

AtMCU1 Localizes to the Mitochondria in Arabidopsis Cells and Is Highly Expressed in the Root

To gain insight into the place of action of the MCU channel, we explored where AtMCU1 is located within the plant cell. According to the consensus targeting prediction, five of six Arabidopsis isoforms are expected to be located in the mitochondria despite N-terminal sequences that differ markedly both in length and amino acid sequence, while only one is predicted to reside in the plastids (Supplemental Table S1). On the other hand, ChloroP1.1 predicts plastidial localization of another two isoforms with a probability score higher than 0.5. These bioinformatic predictions need experimental validation, since a dual localization to the plastids and the mitochondria may arise from ambiguous signal sequences (Karniely and Pines, 2005). In addition, even unambiguous predicted signals have been found incorrect following experimental validation in several studies (e.g. Carraretto et al., 2016).

The Aramemnon database (Schwacke et al., 2003) predicts a clear mitochondrial targeting for AtMCU1, but empirical evidence has been lacking. We generated an AtMCU1:GFP fusion construct under the control of a *35S* promoter, which we expressed transiently in Arabidopsis leaf epidermal cells by *Agrobacterium tumefaciens* infiltration. Confocal microscopy analysis indicated that the GFP signal did not colocalize with chloroplast autofluorescence (Fig. 4A) but with highly motile cytoplasmic structures (Video 1). Furthermore, AtMCU1:DsRed2 colocalized with a mitochondrial GFP marker that employs the presequence of the β-subunit of ATP synthase (Logan and Leaver, 2000; Fig. 4B).

Next, we analyzed expression of the *AtMCU1* transcript in different tissues of four-week-old wild-type plants (ecotype Col-0) by quantitative RT-PCR (Fig. 4C). We detected the highest expression in root tissue, consistent with public data from Affymetrix Arabidopsis ATH1 Genome Array (http://genSisible.com/tissues/AT/AGI/AT1G09575). Intermediate expression was evident in all other tissues tested, with the exception of seeds, where expression was below the detection limit.

Arabidopsis Lines Lacking AtMCU1 Expression Show Altered Root Length and Mitochondrial Ultrastructure

To assess the functional role that AtMCU1 plays at the whole plant level, we made use of two lines with T-DNA insertions in the *AtMCU1* locus. Both publically available lines were tested for antibiotic resistance, presence of the T-DNA insertion, and abundance of *AtMCU1* transcript. Based on that, the homozygous lines of N582151 (SALK_082151.43.80.x; *mcu1-1*) and GK-035G08 (*mcu1-2*) were confirmed as knockouts in which the *AtMCU1* transcript was undetectable (Fig. 5, A and B).

Given the observed high expression of *AtMCU1* in root, we hypothesized that functional alterations are most likely to affect the root. Here, mitochondria are the prime site of energy conversion underpinning growth and development (Atkin and Macherel 2009; Pu et al., 2015). Blue-native PAGE indicated that no gross alterations occur in the mutants regarding the assembly of respiratory chain complexes (Fig. 5C), unlike in insulin-secreting mammalian cells, where knockdown of MCU resulted in decreased respiratory chain protein levels (Quan et al., 2015). In seedlings grown on 1% (w/v) Suc, root length (Supplemental Fig. S3A) and respiratory characteristics of isolated mitochondria (Supplemental Fig. S3, B–D) were comparable to that observed in Col-0 plants. However, when seedlings

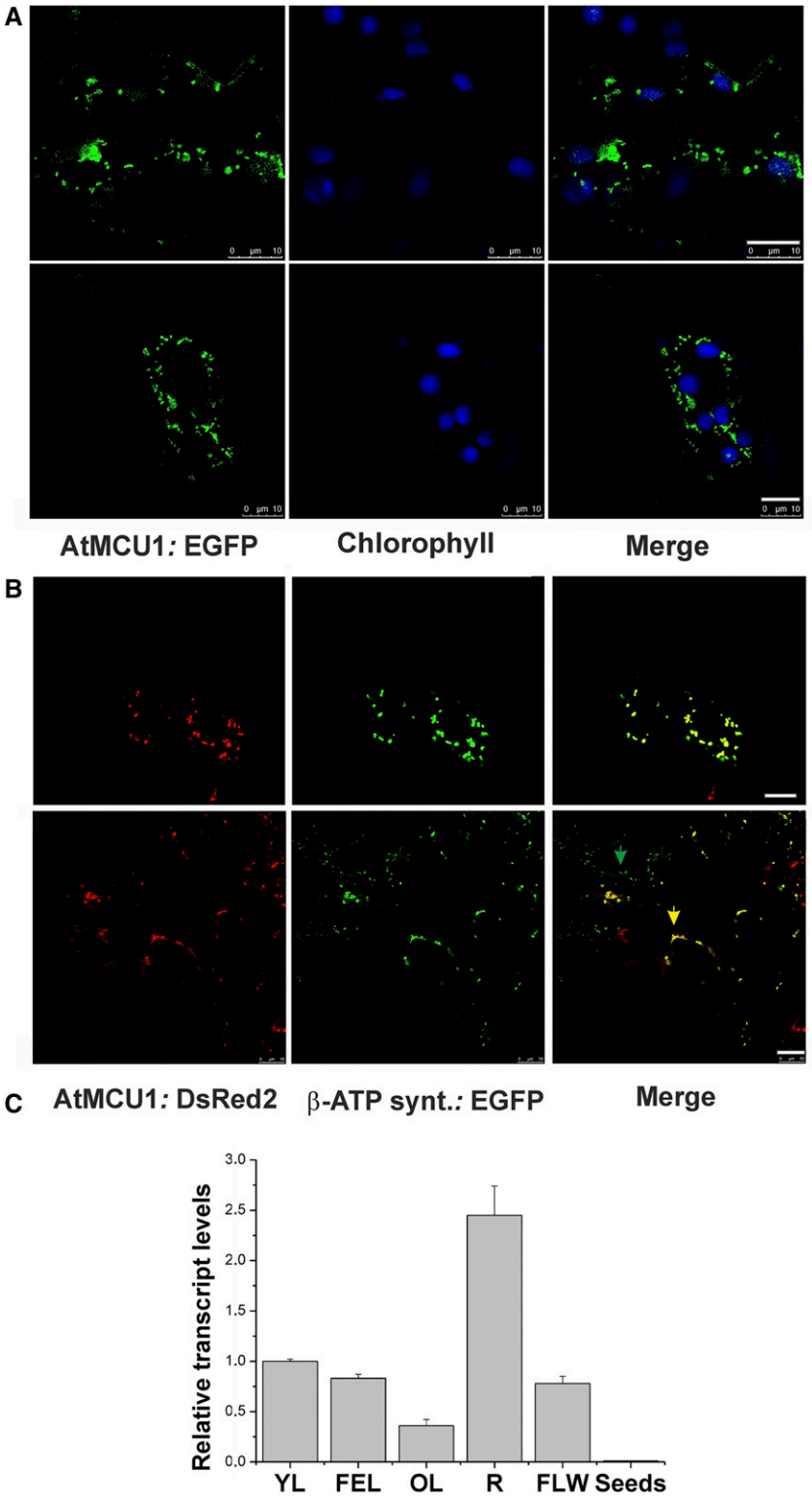

Figure 4. AtMCU1 localizes to mitochondria. A, EGFP signal (green) in Arabidopsis leaf cells transiently expressing a *2×35S:AtMCU1:EGFP* construct. Chlorophyll autofluorescence is shown in blue. B, Colocalization between transiently expressed AtMCU1:DsRed2 and a stably expressed EGFP targeted to the mitochondria (Logan and Leaver, 2000). Cells positive for the mitochondrial marker only (green arrow) and for both signals (yellow arrow) in the same leaf area are visible. Representative images from two of three independent experiments are shown in A and B. Scale bar = 10 μm. C, *AtMCU1* expression in different plant tissues (n = 3, mean values ± SD). Transcript levels relative to *Actin2* in young leaves (YL) are shown. FEL, fully expanded leaves; FLW, flowers; OL, old leaves; R, roots; Seeds, imbibed seeds.

were grown on 0.1% (w/v) Suc, the primary root length of the plants from both lines (*mcu1-1* and *mcu1-2*) lacking AtMCU1 was significantly and reproducibly shorter than that of Col-0 plants 10 d after germination (Fig. 5D). Likewise, mitochondrial morphology and cristae formation as observed by transmission electron microscopy analysis were different in the roots of 2-week-old *mcu1-1* and *mcu1-2* plants as compared to Col-0. In the wild-type control, the majority of mitochondria exhibited normal ultrastructure, with

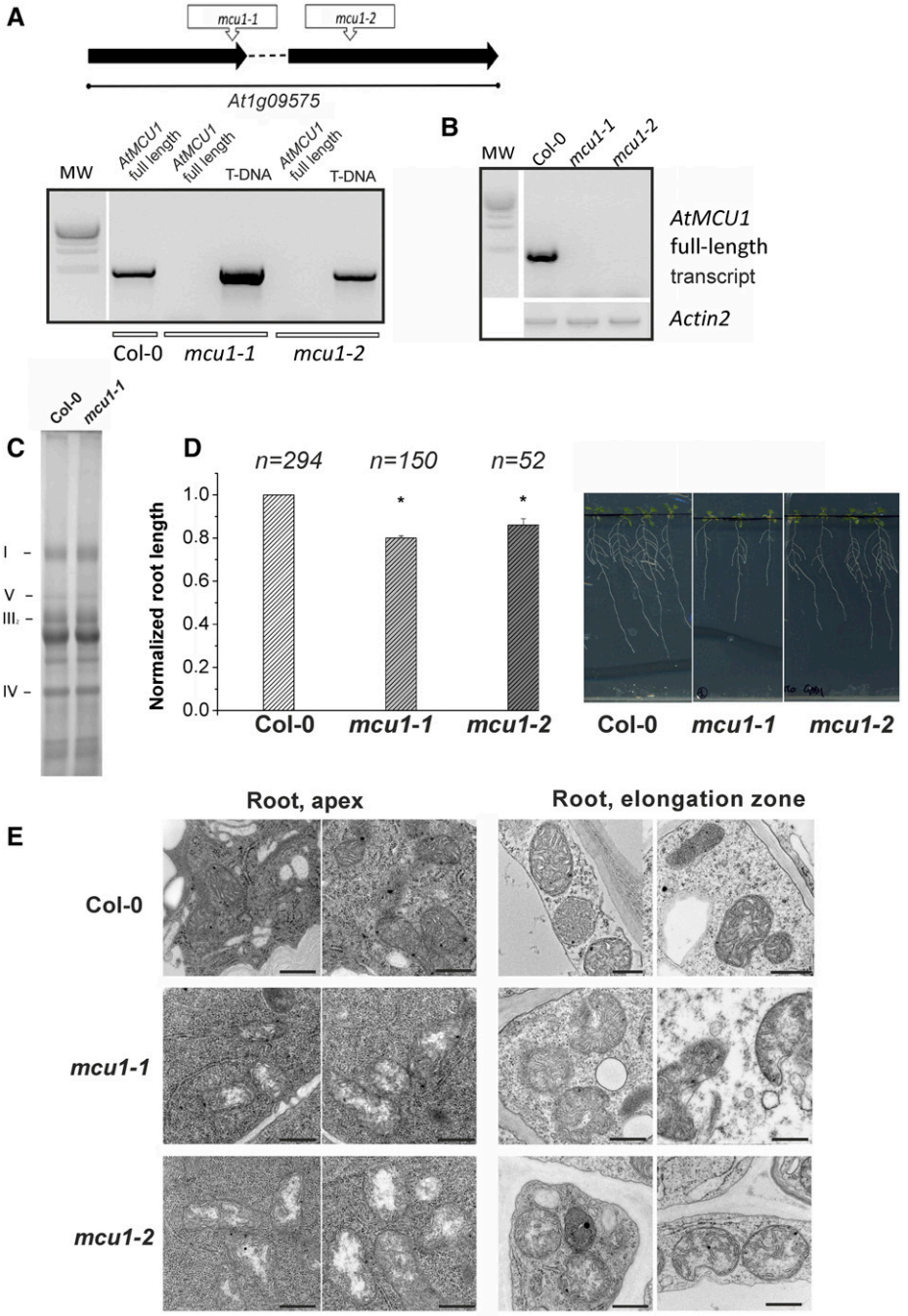

Figure 5. Characterization of Arabidopsis seedlings lacking AtMCU1. A, Positions of T-DNA insertions in the *AtMCU1* gene model are indicated for lines *mcu1-1* and *mcu1-2*. Middle: genotyping of the T-DNA insertions in two T-DNA insertion lines for the *AtMCU1* locus. B, *AtMCU1* transcript analysis in *mcu1-1* and *mcu1-2* by semiquantitative PCR relative to *Actin2*. One-kilobase step ladder (Promega) was used as molecular weight (MW) marker (from 1 to 10 kb). C, Respiratory chain complexes, separated by BN-PAGE. D, Quantification of primary root length in the Col-0, *mcu1-1*, and *mcu1-2* lines from 4 to 10 independent experimental replicates (20 replicates for Col-0). $*P \leq 0.01$ (Student's *t* test). For each mutant line, the root length was normalized with respect to the mean value obtained from Col-0 in the same experimental replicate. Error bars = ±SD. Representative images of seedlings used for quantification of root length 10 d after germination and grown on media supplemented with 0.1% (w/v) Suc. E, Transmission electron micrographs of mitochondria from two independent experiments. Top and bottom rows show exemplary images from Col-0 and *mcu1-1* and *mcu1-2* knockout plants in the apical root and the elongation zone. A quantification is provided in Figure 7C. Scale bars = 500 nm.

electron-dense, uniform matrix filled with cristae in both the elongation and the apical zones. In the plants lacking AtMCU1, a higher proportion of mitochondria displaying altered shape and cristae organization was present (Fig. 5E; Supplemental Fig. S4A). The number and dimension of mitochondria using MitoTracker Orange CMTMRos in roots of 10-d-old seedlings were also compared without showing obvious changes (Supplemental Fig. S4B). Together, these results suggest that a part of the mitochondrial population is affected by the lack of AtMCU1 that manifests in a root developmental defect under specific growth conditions. Since AtMCU1 is expressed also in the shoot and an interplay between mitochondrial and chloroplast function might occur (Lee et al., 2008; Weber and Linka 2011; H.P. Braun et al., 2014; Kmiecik et al., 2016), we characterized rosette size (Supplemental Fig. S5A) and photosynthetic efficiency (Supplemental Fig. S5B) without revealing any significant differences. According to eFPBrowser (http://bbc.botany.utoronto.ca/efp/cgi-bin/efpWeb.cgi?primaryGene=At1g09575&modeInput=Absolute), *AtMCU1* is highly expressed also in the mature

pollen, yet we did not observe any impact on seed production in the mutant plants.

In Vivo Measurements of Mitochondrial Ca^{2+} Accumulation in Root Tips of Mutant Plants Reveal Slight Changes in Ca^{2+} Dynamics

Given the Ca^{2+}-permeable channel activity of recombinant AtMCU1 in vitro, we compared the mitochondrial Ca^{2+} uptake dynamics in seedling roots from 1-week-old Col-0 and mutant plants grown in 0.1% (w/v) Suc. We crossed Col-0 and *mcu1-1* plants with Col-0 plants harboring the mitochondria-targeted, genetically encoded Ca^{2+} probe Yellow Cameleon YC3.6 (Loro et al., 2012). To induce Ca^{2+} transients in the mitochondrial matrix, Col-0 and *mcu1-1* seedlings were treated with 0.1 mM external ATP as previously described (Teardo et al., 2015; Wagner et al., 2015). Mitochondrial Ca^{2+} uptake upon stimulation occurred in both genotypes, with mild but statistically significant differences in the kinetics of accumulation and of release (Fig. 6, A–F). A comparison of resting free Ca^{2+} concentrations in the matrix between both genotypes did not show significant differences. Overall, in these young roots, only slight differences in mitochondrial Ca^{2+} dynamics could be observed, suggesting that other, mitochondria-targeted AtMCU isoforms or alternative Ca^{2+} uptake systems compensate for loss of AtMCU1. Indeed, quantitative RT-PCR analysis showed expression of other homologs in the root, with *At4g36820* (AtMCU4) showing the highest transcript levels (Supplemental Fig. S6A). Transient expression of *2×35S:AtMCU4:EGFP* in Arabidopsis leaf epidermis revealed mitochondrial targeting also for this homolog (Supplemental Fig. S6B).

Arabidopsis Lines Overexpressing AtMCU1 Show Altered Root Length and Mitochondrial Ultrastructure

The above experiments indicate an efficient backup by additional AtMCU homologs in vivo. Yet, mitochondria isolated from seedlings lacking AtMCU1 in two independent lines display altered ultrastructure and root length, suggesting that the absence of AtMCU1 cannot be fully compensated for by other AtMCU isoforms at all levels, leading to a general acclimation of mitochondrial function. To assess the consequences of MCU overexpression in intact plants, we generated four independent stable Arabidopsis lines, with high *AtMCU1* transcript levels in the Col-0 and the *mcu1-1* backgrounds (Fig. 7A). Expression of *35S:MCU1:GFP* in root mitochondria was confirmed by confocal microscopy (Fig. 7B). Surprisingly, increased expression of the protein led to similar changes as its absence, that is to decreased root length in comparison to Col-0 (Fig. 7C) and altered mitochondrial ultrastructure (Fig. 7, D and E), indicating a gene-dose effect that leads to mitochondrial stress both upon decreased and increased expression of AtMCU1.

Since changes in the composition of respiratory chain complexes could not be detected and respiratory capacity was maintained, it appears unlikely that the observed growth defect was due to impaired bioenergetic efficiency in the knockout plants. A hypothetical link between MCU expression and root development is represented by reactive oxygen species (ROS) dynamics, since maintenance of ROS homeostasis has been suggested to be critical for normal plant development. MCU overexpression in *Trypanosoma* was correlated with increased rates of ROS generation (Huang et al., 2013). On the contrary, lack of functional MCU was

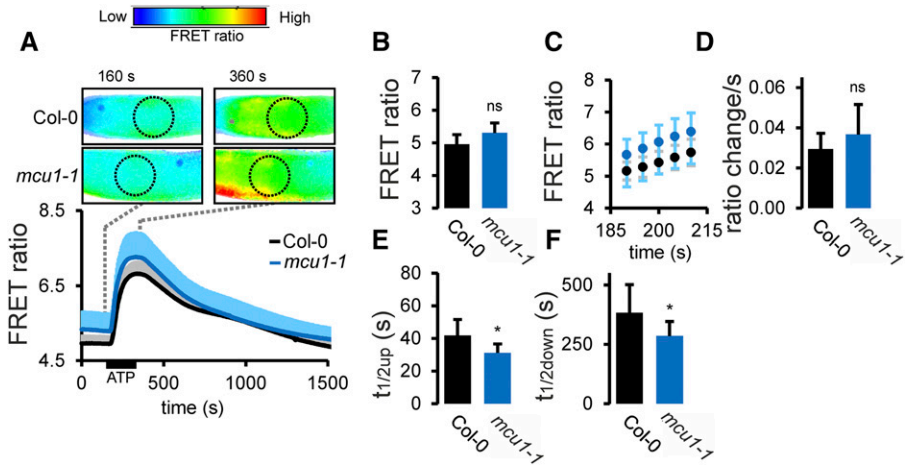

Figure 6. The dynamic properties of mitochondrial Ca^{2+} transients in *mcu1-1* and wild-type plants. A, Wild-type control (Col-0) and *mcu1-1* plants were imaged for 175 s before being treated with 0.1 mM extracellular ATP that was removed after another 180 s. FRET ratio changes were analyzed in a defined region of interest (dotted circle). B, Steady-state FRET ratios were calculated in a 35-s time frame directly preceding the application of ATP. C, Linear FRET ratio increase following ATP application. D, Slope of a regression line through data points shown in C. E, Time to reach half-maximal FRET ratio after the application of stimulus. F, Time to pass half-maximal ratio while recovering from maximal FRET ratio. $n \geq 7$; error bars = SD; $^*P \leq 0.05$.

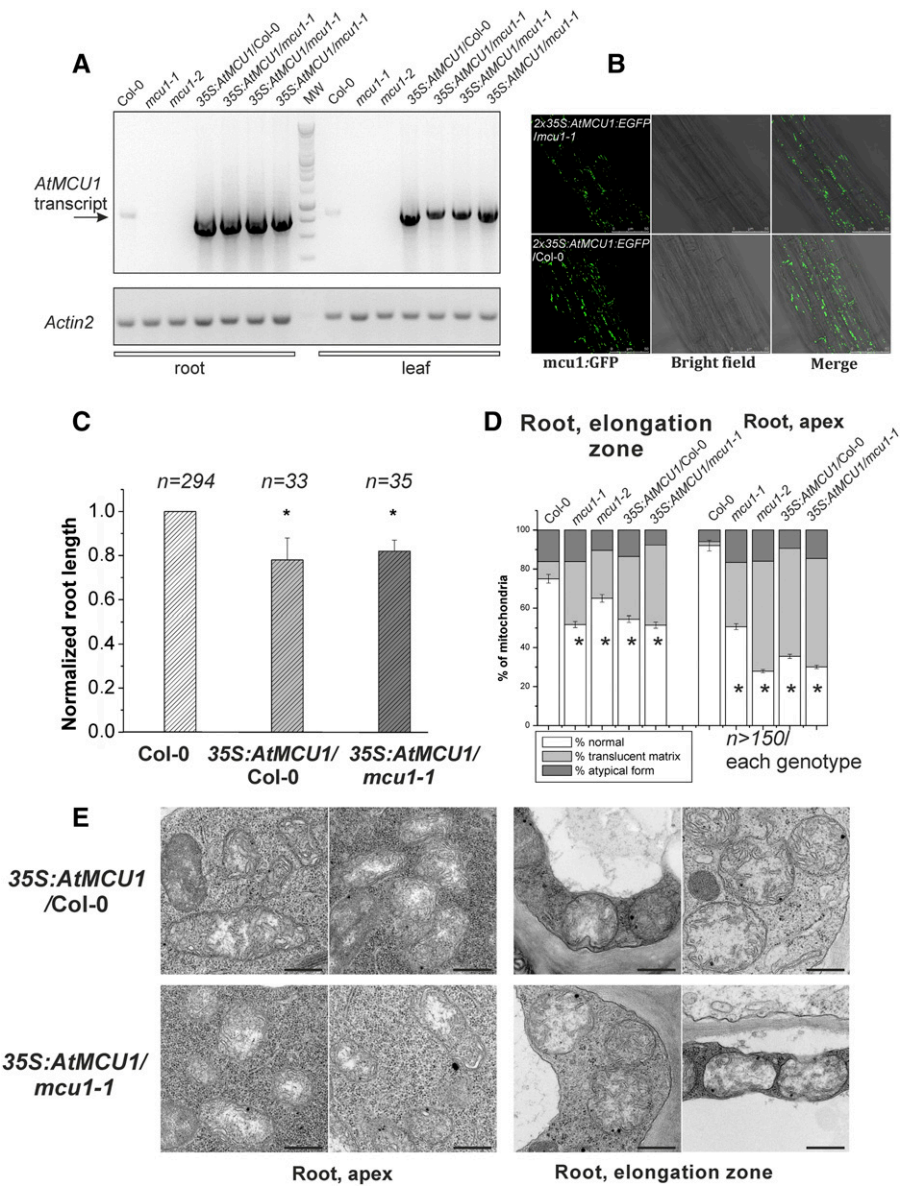

Figure 7. Characterization of Arabidopsis lines overexpressing *AtMCU1*. A, *AtMCU1* transcript analysis by semiquantitative PCR in Col-0, *mcu1-1*, and *mcu1-2* and lines overexpressing *AtMCU1* either in Col-0 background (*35S:AtMCU1/Col-0*) or in *mcu1-1* background (*35S:AtMCU1/mcu1-1*). One-kilobase ladder (Promega) was used as molecular weight (MW) marker (from 250 to 1000 bp). B, Confocal images of *2×35S:AtMCU1:EGFP* expressing lines confirm the presence of AtMCU1 in root mitochondria. Representative images of two experiments are shown. C, Data are from ≥4 independent experimental replicates. $*P \leq 0.01$ (Student's *t* test). D, Percentage of mitochondria with normal ultrastructure or with translucent matrix of atypical form in the apex and elongation zones of roots from the different lines. ≥150 mitochondria were assessed per line, deriving from three seedlings for each genotype. Statistical analysis revealed significant differences ($P \leq 0.05$; Student's *t* test) in all lines with respect to Col-0 regarding the percentage of abnormal mitochondria. E, Transmission electron micrographs of mitochondria from two independent experiments. Exemplary images from three different plants/genotype in the apical root and the elongation zone. A quantification is provided in Figure 7D. Scale bars = 500 nm.

found to modestly decrease mitochondrial ROS production and to trigger transcriptional reprogramming (Rasmussen et al., 2015). Unfortunately, however, reliable techniques to measure mitochondrial ROS dynamics in vivo in plants are not available (Jia, 2011; Huang et al., 2016; Tsukagoshi, 2016), and thus, any mechanistic relationship between mitochondrial ROS dynamics and root growth regulation is currently lacking. Yet, both excessive ROS production (Jardim-Messeder et al., 2015) and decreased ROS production rates have been suggested to impair root growth (Foreman et al., 2003; Tsukagoshi et al., 2010). For example, lack of superoxide-producing NADPH oxidase led to a 20% decrease of root length (Foreman et al., 2003), which is within a similar range as the 10% to 22% decrease we observed in the different lines. In our case, an estimate of basal ROS production rates, as measured using the nonfluorescent dihydrorhodamine 123 (DHR123) that becomes oxidized to fluorescent rhodamine 123 by H_2O_2 (Fester and Hause 2005; although not necessarily specifically) was not significantly altered in AtMCU1 knockout or overexpressing roots (Supplemental Fig. S7). Hence, the hypothesis of altered ROS dynamics remains to be addressed in future work. Finally, we analyzed the root apical meristem by propidium iodide staining, which allows the imaging of the walls of living cells. No obvious difference is noticeable between different genotypes in the meristematic zone (Supplemental Fig. S8). Cortex, endodermis, epidermis initials, and quiescent center are detectable in all the analyzed roots, suggesting that auxin and cytokinin signaling pathways that play an important role in controlling the balance between cell division and differentiation in the root meristem (Dello Ioio et al., 2008)

remain functional in the knockout or overexpressor plants.

DISCUSSION

Our work provides experimental evidence for the mitochondrial localization of a plant MCU homolog and its function as a bona fide, RR-sensitive Ca^{2+} channel. It further provides insight into the physiological role that AtMCU1 plays at the whole plant level as investigated by deletion and overexpression in Arabidopsis.

Homologs of the mammalian MCU family in Arabidopsis include six members, of which five have predicted mitochondrial targeting (Stael et al., 2012). However, organelle localization predictions require rigorous empirical validation, particularly in plants where mitochondrial and chloroplast targeting sequences can be very similar (see e.g. Karniely and Pines, 2005; Carraretto et al., 2016). Here we validate that two of six AtMCUs (AtMCU1 and AtMCU4) indeed localize only to mitochondria in intact Arabidopsis plants and display particularly high expression in roots. Independent experimental evidence for localization of AtMCU1-3 to mitochondria has also been obtained (Carraretto et al., 2016; Wagner et al., 2015; Senkler et al., in press). Whether the functional properties of the homologs expressed in the different tissues are the same remains unknown. Sequence alignment between Arabidopsis MCU homologs and those of *H. sapiens* and *C. elegans* highlights that the overall sequence similarity between plant and animal MCUs is relatively low (<25% pairwise sequence identity; Supplemental Fig. S9). Empirical investigation of the electrophysiological properties, as done in this work, is therefore a critical step and one that has been largely missing for MCU proteins in other organisms than mammals. The conserved nature of the selectivity filter region and of the Ser residue responsible for sensitivity to RR in all six Arabidopsis isoforms suggests that AtMCU1 is representative also for the other AtMCUs and that functional insights on the ability of AtMCU1 to form a channel may be, with appropriate caution, extrapolated to the entire AtMCU family.

The recently elucidated structural properties of MCU from *C. elegans* (Oxenoid et al., 2016) allow several considerations: relatively few amino acids are conserved in Arabidopsis MCUs in the regions proposed to be important for the regulation of the *C. elegans* channel (Supplemental Fig. S9). In particular, it was hypothesized that the outer and inner juxtamembrane helices as well as the loop region L2 are unstable regions undergoing conformational changes upon activation by EMRE to create the lateral exit path for Ca^{2+} (Oxenoid et al., 2016). The proposed role of EMRE in mammals also includes mediating the physical interaction between MCU and a MICU1/MICU2 dimer and regulating MCU channel activity depending on the matrix Ca^{2+} concentration (Sancak et al., 2013; Vais et al., 2016). Homologs of EMRE are not present in plants, fungi, or protozoa, and it has been recently shown that EMRE is required for Ca^{2+} uptake in the case of mammalian MCU, but not of MCU from *Dictyostelium discoideum* (Kovács-Bogdán et al., 2014). Likewise, our data indicate that in plants, MCU together with the MICU regulator represents a functional configuration of the MCUC. Indeed, in our electrophysiological experiments, Arabidopsis MICU had a direct effect on AtMCU1. At the level of the above-indicated regions, the amino acid sequence is more similar between Arabidopsis and Dictyostelium than between AtMCUs and human MCU (Supplemental Fig. S10). Highly conserved amino acids (with still unknown specific roles) among all MCUs include an Ile in outer juxtamembrane helices, a Thr in inner juxtamembrane helices, and a Phe in L2, whereas an (R/K)/Q/(R/K)/(K/R)/L motif in the L2 region is characteristic of plant and Dictyostelium MCUs (Supplemental Fig. S10). In principle, this positive charge-rich region might promote the exit of Ca^{2+} by electrostatic repulsion (i.e. without the need of EMRE).

Here, we provide evidence that AtMCU1 gives rise to a channel activity strongly resembling the key characteristics of animal MCU, despite the low overall amino acid identity with the mammalian MCU protein. A characteristic feature of Ca^{2+} channels is mediation of Na^+ flux when divalent cations are present at very low concentrations (10 pM, as compared to 100 mM Na^+). However, under physiological conditions, Ca^{2+} will pass through the channel given that it binds Ca^{2+} with high affinity (Kirichok et al., 2004). The observed inhibitory effect of MICU on channel activity at low Ca^{2+} concentration (the steady-state free Ca^{2+} is in the range of 100 nM in the Arabidopsis cytosol; Stael et al., 2012) is in accordance with the gatekeeper function of Arabidopsis MICU under basal conditions and with the increased basal matrix Ca^{2+} concentration in mitochondria lacking MICU (Wagner et al., 2015). The system we used for the electrophysiological studies is highly suitable to gather definitive evidence as to whether a protein can form an ion channel. Patch clamp, which may be regarded as an alternative for organelle-located ion channels, is technically extremely challenging for plant mitochondria and has been performed on wheat germ mitochondria only (De Marchi et al., 2010), while no successful application has been reported for Arabidopsis mitochondria yet.

Since the discovery that mitochondria are able to accumulate Ca^{2+}, fundamental roles in regulating mitochondrial physiology, energy metabolism, and cell fate have been associated with Ca^{2+} dynamics, with a majority of this work based on animal systems (Wagner et al., 2016). As to plant mitochondria, Ca^{2+} uptake into isolated mitochondria has been observed in different systems for decades, but critical uncertainties about the mechanism (uniport versus symport with phosphate) have remained (e.g. Martins and Vercesi, 1985; Silva et al., 1992; Zottini and Zannoni, 1993; Virolainen et al., 2002). Since oxidative phosphorylation is based on an electrochemical gradient across the inner mitochondrial membrane, ion channels in this membrane may be

expected to impact the regulation of energy metabolism (e.g. Szabò and Zoratti, 2014). Indeed, genetic manipulation of MCU in several organisms resulted in energetic defects especially under stress conditions, as demonstrated in zebrafish (Prudent et al., 2013) and in *Trypanosome brucei* (Huang et al., 2013), where, like in mammals, only a single active channel-forming isoform is present. Genetic ablation of MCU in the germline of mice, however, displayed only a mild phenotype, possibly due to compensation at the system level (Pan et al., 2013; Murphy et al., 2014). On the other hand, postnatal silencing or overexpression of MCU clearly demonstrated that MCU expression triggers muscle hypertrophy, both during postnatal growth and in adulthood, by affecting retrograde signaling (Mammucari et al., 2015). Furthermore, the importance of correct mitochondrial Ca^{2+} handling is emphasized by a human disease associated with mutation of MICU1 (Logan et al., 2014) and by the requirement of MICU1 for adaptation to postnatal life and for tissue repair after injury (Antony et al., 2016). Interestingly, both MCU-overexpressing and MCU-silenced muscle fibers harbored atypical mitochondria with altered cristae structure and severely damaged mitochondria with disrupted cristae (10% of total), although such ultrastructural changes were not associated with an overall metabolic dysfunction (Mammucari et al., 2015). Here we show that a similar situation is found in Arabidopsis, where both lack and overexpression of AtMCU1 caused appearance of mitochondria with irregular shape, alteration of cristae, and partial loss of matrix density. The fact that we observed these changes in two independent knockout lines as well as in wild-type plants overexpressing the protein indicates that this morphological change is intimately linked to alteration of the Ca^{2+} channel expression. The exact mechanism accounting for this link is unclear, but the lack of another putative Ca^{2+}-flux mediator, the Glu receptor 3.5 in mitochondria, as well as of the AtMCU regulator MICU equally correlated with severe morphological changes (Teardo et al., 2015; Wagner et al., 2015). Taken together, these data suggest a link between mitochondrial Ca^{2+} and organelle biogenesis and/or morphology by a mechanism that still awaits clarification in both animals and plants.

Previous work has already suggested that in plants, mitochondrial function is important for root growth, which may be due to their strict dependence on respiratory energy provision (de Longevialle et al., 2007; Huang and Millar, 2013). In this study, modifying MCU1 expression significantly impacted root growth under restrictive carbon source availability, without obvious changes in ROS dynamics or in organization of the meristematic zone. Future work is required to clarify whether the observed root phenotype is directly related to a relatively low percentage of structurally abnormal mitochondria and/or, similarly to muscle, to altered Ca^{2+}-mediated downstream signaling.

In summary, our work clearly shows that plants possess a functional mitochondrial uniporter system. It provides a comprehensive functional characterization of AtMCU1, a plant homolog of the mammalian calcium uniporter, unraveling conserved but also distinct properties. It identifies a plant-specific phenotype in the absence and overexpression of one AtMCU isoform, raising the question about specific and redundant roles of plant MCU protein family for future studies. As such, it paves the way to investigate the physiological importance of mitochondrial Ca^{2+} regulation in plants.

MATERIALS AND METHODS

Phylogenetic Analysis

Human MCU (UniProt ID: Q8NE86) was used to retrieve sequences of plant homologs from https://phytozome.jgi.doe.gov/pz/portal.html through a BLASTP search. Sequences from selected species (Supplemental Fig. S1) were iteratively aligned with MUSCLE (Curtis and Grossniklaus, 2003), manually cured, and used to calculate a phylogenetic tree using MrBayes (Huelsenbeck and Ronquist, 2001). A Markov chain Monte Carlo simulation was run for 2,000,000 generations with three chains under mixed amino acid models.

In Vitro Expression of AtMCU and ΔMICU

AtMCU1 protein was expressed in an in vitro wheat (*Triticum aestivum*) germ lysate system based on the continuous exchange cell-free technique, using the RTS 100 Wheat Germ CECF Kit (Roche). Synthesis was conducted for 24 h at 24°C under continuous mixing on a Thermomixer comfort unit (Eppendorf). After expression, the reaction mixture (30 μL) was directly solubilized for 30 min at room temperature with one of six different detergents (Triton X-100, SDS, β-DDM, decyl-β-D-maltopyranoside *n*-octyl β-D-glucopyranoside, and CHAPS) added to 2% (w/v). After centrifugation, the supernatant containing the solubilized proteins selected for electrophysiological characterization was diluted 1:10 in 10 mM HEPES, pH 7.4, and then used in planar lipid bilayer experiments.

The *ΔMICU* sequence (*At4g32060*) was cloned into pET28a vector fused to a 6×His tag for expression into *Escherichia coli* cells. After induction of protein expression, a HisTrap HP column (GE Healthcare) was used to purify ΔMICU protein as described previously (Wagner et al., 2015).

SDS-PAGE and BN-PAGE

SDS-PAGE was performed in the presence of 6 M urea (Carraretto et al., 2013), and western blotting was carried out as described previously (Teardo et al., 2011). Protein complex analyses were conducted on blue native-PAGE (BN-PAGE). Protein complexes from purified mitochondria were solubilized in the presence of 1.5% (w/v) *n*-dodecyl-maltoside, 375 mM 6-aminohexanoic acid, 250 mM EDTA, and 25 mM Bis-Tris, pH 7.0. Solubilized protein complexes were centrifuged at 15,000*g* and 4°C for 20 min, and 1% (w/v) Coomassie Brilliant Blue G was added to the supernatant prior to separation by electrophoresis on a 4% to 12% acrylamide gradient BN gel as described previously (Larosa et al., 2012).

Bilayer Experiments

An asolectin solution in decane/chloroform with a 100:1 ratio per mg of lipids was used for artificial membrane construction. A membrane of 100 mV/pF was constructed between two compartments (cis/trans), and 3 mL of Na-gluconate (low-divalent cation medium, 100 mM Na-gluconate, 5 mM EDTA, and 10 mM HEPES, pH 7.4) or $CaCl_2$ (100 mM $CaCl_2$ and 10 mM HEPES, pH 7.4) or Ca-gluconate (100 mM Ca-gluconate and 10 mM HEPES, pH 7.4) were added to the cis and trans compartments. Then 10 μL of the solubilized and diluted AtMCU1 prepared as in Raffaello et al. (2013) was added to the cis side. Control experiments ($n = 50$) showed no activity without addition of the protein. $GdCl_3$ or RR was added to both compartments to the required concentration for inhibition assays. Then 10 μL of purified ΔMICU protein was added (100 ng/mL) to both sides. Analysis of data was performed using the PCLAMP8.0 and Origin 6.1 programs (for Gaussian and linear fitting).

Plant Material and Growth Conditions

Arabidopsis (*Arabidopsis thaliana*) plants were grown under controlled conditions: 22°C, long-day photoperiod (16 h light, 8 h dark), 90 μmol photons m^{-2} s^{-1}, 70% relative humidity. Seeds were surface-sterilized with hypochlorite, incubated for 2 d at 4°C in the dark, and allowed to germinate in half-strength Murashige and Skoog (MS; Duchefa) medium solidified with 0.8% (w/v) plant agar. Seedlings were picked and transferred to soil. For measurement of root length and MitoTracker Orange CMTMRos staining, surface-sterilized seeds were grown on vertical culture plates containing half-strength MS medium supplemented with 0.1 or 1% (w/v) Suc and 0.8% (w/v) plant agar for 10 d.

Mutant Genotyping, Construct Preparation, and Plant Transformation

Two independent T-DNA insertion lines for the *At1g09575* locus were obtained from NASC (European Arabidopsis Stock Centre): SALK_082151 from the SALK collection and GK-035G08 from GABI-Kat collection. Total genomic DNA was extracted from each line following standard procedures: after extraction, the full-length gene sequence was PCR-amplified with a specific primer for the T-DNA construct and the other on *At1g09575* to confirm the position of T-DNA in the AtMCU1 gene sequence (SALK and GK specific primers; Supplemental Table S2).

RNeasy Plant Mini kit (Qiagen) was used to extract total RNA from Arabidopsis mutant leaves: 5 μg of RNA was reverse-transcribed with the SuperScriptII Reverse Transcriptase (Invitrogen). Primers AtMCU1.1_for and AtMCU1.1_rS and ACTRT_for and ACTRT_rS (Supplemental Table S2) were used for the full-length *AtMCU1* and the *Actin2* (*At3g18780*) control transcript.

The *At1g09575* coding sequence was amplified by using the following primers: AtMCU1.1_for and AtMCU1.1_rS and AtMCU1.2_for and AtMCU1.2_rS (Supplemental Table S2). PCR products were digested with *Nde*I/*Sac*I (NEB Biolabs) for ligation into pIVEX1.4WG (Roche) and *Pst*I/*Sma*I (NEB Biolabs) for ligation into pGREAT:EGFP. The *At4g36820* coding sequence was also PCR-amplified (primers listed in Supplemental Table S2) and ligated into pGREAT:EGFP for localization studies. Transient expression was performed as in Carraretto et al. (2013).

For stable overexpression of *At1g09575*, Arabidopsis plants (Col-0 and SALK_082151) were transformed by floral dip with *Agrobacterium tumefaciens* GV3101, carrying the pGREAT- *2×35S:AtMCU1:EGFP* construct in the presence of pSoup.

Quantitative RT-PCR

RNA was extracted from seeds imbibed in water for 24 h, from flowers of 6-week-old plants, and from leaves and roots of 4-week-old plants, using the RNeasy Plant Mini kit. Reverse transcription was performed with 100 ng^{-1} μg RNA (SuperScript II Reverse Transcriptase; Life Technologies). Quantitative RT-PCR was performed using GoTaq qPCR Master Mix (Promega) in an AB Applied Biosystems 7500 Real-Time PCR System, by using the following primer pair: AtMCU1_qPCR_for and AtMCU1_qPCR_rS (Supplemental Table S2). *Actin2* (*At3g18780*) was amplified as the reference gene using the following primer pair: Act_qPCR_for and Act_qPCR_rS. Data were analyzed by the $\Delta\Delta C_t$ method (Livak and Schmittgen 2001).

MitoTracker Staining of Root Mitochondria

Ten-day-old seedlings were incubated in 500 nM MitoTracker Orange in half-strength MS medium for 15 min and rinsed for 15 min in dye-free medium before imaging.

Confocal and Transmission Electron Microscopy

Images were collected with a Leica TCS SP5 II confocal laser scanning microscope (Leica Microsystems) with 40× HCX PL APO CS (1.25–0.75 numerical aperture) oil-immersion objective. Laser lines at 488 and 543 nm were used for excitation of EGFP and MitoTracker Orange/DsRed2, respectively. Emission paths were 505 to 525 nm for EGFP, 570 to 620 nm for MitoTracker Orange, 560 to 580 nm for DsRed2, and 680 to 720 nm for chlorophyll autofluorescence. Transmission electron micrographs were obtained from 2-week-old Arabidopsis plants as described in Carraretto et al. (2013).

Root and Rosette Measurements

Measurements of root length were done by using ImageJ software (W.S. Rasband, ImageJ, U.S. National Institutes of Health). For the evaluation of rosette size, plants were sown onto soil and grown in individual pots. The Leaf Lab tool (Version 1.41) provided by Mark D. Fricker was used to assess the leaf area (Fricker, 2016).

Seedling Preparation for Ca^{2+} Imaging

Arabidopsis seeds were surface-sterilized by vapor-phase sterilization and plated on half-strength MS medium supplemented with 0.1% (w/v) Suc and 2.34 mM MES, pH 5.8 and solidified with 0.8% (w/v) of plant agar. After stratification at 4°C in the dark for 3 d, seeds were transferred to the growth chamber with 16-/8-h cycles of light (70 μmol photons m^{-2} s^{-1}) at 22°C. The plates were kept vertically. Seedlings used for the analyses were 7 to 8 d old, which corresponds to an average root length of 3 cm. For root cell imaging, the seedlings were prepared according to Behera and Kudla (2013) in dedicated chambers and overlaid with wet cotton to continuously perfuse the root with the imaging solution (5 mM KCl, 10 mM MES, and 10 mM $CaCl_2$, pH 5.8 adjusted with Tris). The shoot was not submerged in the solution, and in order to prevent possible artifacts linked to the specimen manipulation, we routinely kept the seedlings for 10 min in continuous solution perfusion before the start of the recordings. ATP (final concentration of 0.1 mM) was added as disodium salt to the chamber by perfusion with the same solution. ATP was perfused for 3 min and then washed out.

Time-Lapse Ca^{2+} Imaging Analyses

Seedling roots expressing the mitochondrial localized Yellow Cameleon 3.6 (Loro et al., 2012) were imaged in vivo by an inverted fluorescence microscope Nikon Ti-E (Nikon) with a CFI PLAN APO 20× VC dry objective. Excitation light was produced by a fluorescent lamp Prior Lumen 200 PRO (Prior Scientific) at 440 nm (436/20 nm) set to 20%. Images were collected with a Hamamatsu Dual CCD Camera ORCA-D2 (Hamamatsu Photonics). For Yellow Cameleon analysis, the FRET CFP/YFP optical block A11400-03 (emission 1 483/32 nm for CFP and emission 2 542/27 nm for the FRET) with a dichroic 510-nm mirror (Hamamatsu Photonics) was used for the simultaneous CFP and cpVenus acquisitions. Exposure times were 100 ms for roots with a 4 × 4 CCD binning. Images were acquired every 5 s. Filters and dichroic mirrors were purchased from Chroma Technology. The NIS-Element (Nikon) was used as a platform to control microscope, illuminator, camera, and postacquisition analyses. Individual ratiometric images and time lapse imaging data were analyzed using a custom Matlab program (Fricker, 2016) as described recently in detail (Wagner et al., 2015).

Measurement of Photosynthetic Efficiency

Seeds were sown on neutral peat substrate (Jiffy-7; Jiffy Group) and incubated for 2 d at 4°C in the dark. Cultivation was performed at 22°C, 40 μmol photons m^{-2} s^{-1}, long-day 16:8 photoperiod. Fluorescence values were regularly measured (at weeks 3, 4, and 5 after germination) using eight plants per genotype; data shown in the text were recorded after 16 h of light followed by 20 min of dark adaptation. Fluorescence was detected by PAM imaging using FluorCam7 (Photon Systems Instruments) applying a saturation pulse of 5,322 μE m^{-2} s^{-1} for 800 ms in the dark; maximum PSII quantum yield in dark-adapted state = variable fluorescence in dark-adapted state (F_v)/maximum fluorescence in dark-adapted state (F_m).

Respiratory Measurements

Oxygen consumption of isolated mitochondria from Arabidopsis roots was measured as described recently (Wagner et al., 2015). Arabidopsis mitochondria from 2-week-old seedlings were isolated, and oxygen consumption and integrity of the outer mitochondrial membrane were assayed as described by Sweetlove et al., 2007.

Visualization of Root Apical Meristem

Eleven-day-old seedlings, grown on 0.1% (w/v) Suc, were stained with 5 μM propidium iodide (Sigma-Aldrich) for 5 min, then rinsed in milliQ water and mounted on a microscope slide. Root apical meristem was imaged using a Leica

SP5 confocal laser scanning microscope with excitation at 488 nm and emission at 560 to 620 nm. Images were analyzed using ImageJ.

ROS Detection in Root Tips

DHR123 (ThermoFisher Scientific) was dissolved at 5 μM in milliQ water (working solution). Seedlings were incubated for 10 min in 5 μM DHR123, rinsed in milliQ water, mounted on a microscope slide, and observed using a Leica 5000b fluorescence microscope (excitation 485 nm, emission 535 nm, 5× objective).

Accession Numbers

Sequence data from this article can be found in the GenBank/EMBL data libraries under accession numbers AT1G09575 (AtMCU1), AT1G57610 (AtMCU2), AT2G23790 (AtMCU3), AT4G36820 (AtMCU4), AT5G42610 (AtMCU5), AT5G66650 (AtMCU6), AT4G32060 (MICU), and AT3G18780 (ACTIN2).

SUPPLEMENTAL DATA

The following supplemental materials are available.

Supplemental Figure S1. Amino acid sequences of the pore region of MCU homologs from 36 species from the plant kingdom.

Supplemental Figure S2. AtMCU1 is selective for Ca^{2+} over Cl^- and responds to classical inhibitors of mammalian MCU.

Supplemental Figure S3. Lack of AtMCU1 does not alter respiration.

Supplemental Figure S4. Ultrastructure, overall number, and size of mitochondria in *mcu1-1*.

Supplemental Figure S5. The impact of lack of AtMCU1 on growth and photosynthetic efficiency.

Supplemental Figure S6. Expression analysis of the Arabidopsis MCU isoforms and subcellular localization of AtMCU4.

Supplemental Figure S7. Qualitative estimation of ROS production in root tips of plants lacking or overexpressing AtMCU1.

Supplemental Figure S8. Basic structural and developmental features of root tips from plants lacking or overexpressing AtMCU1.

Supplemental Figure S9. Amino acid sequence homology between AtMCU isoforms and MCU from *H. sapiens* and *C. elegans*.

Supplemental Figure S10. Amino acid sequence homology between Arabidopsis MCU isoforms and MCU from *D. discoideum*.

Supplemental Movie. Timelapse of Arabidopsis leaf epidermis imaged after infiltration with *A. tumefaciens* harboring the AtMCU1:GFP construct. For comparison of motility, see also videos of Teardo et al., 2015.

Supplemental Table S1. Predicted targeting and cleavage site for Arabidopsis MCU proteins.

ACKNOWLEDGMENTS

We thank Dr. Laura Cendron for help with the isolation of Arabidopsis ΔMICU and Professors Luca Scorrano, Lorella Navazio, Claire Remacle, and Michela Zottini for useful discussion.

Received August 30, 2016; accepted December 21, 2016; published December 28, 2016.

LITERATURE CITED

Akerman KE, Moore AL (1983) Phosphate dependent, ruthenium red insensitive Ca^{2+} uptake in mung bean mitochondria. Biochem Biophys Res Commun **114:** 1176–1181

Antony AN, Paillard M, Moffat C, Juskeviciute E, Correnti J, Bolon B, Rubin E, Csordás G, Seifert EL, Hoek JB, Hajnóczky G (2016) MICU1 regulation of mitochondrial Ca^{2+} uptake dictates survival and tissue regeneration. Nat Commun **7:** 10955

Atkin OK, Macherel D (2009) The crucial role of plant mitochondria in orchestrating drought tolerance. Ann Bot (Lond) **103:** 581–597

Baughman JM, Perocchi F, Girgis HS, Plovanich M, Belcher-Timme CA, Sancak Y, Bao XR, Strittmatter L, Goldberger O, Bogorad RL, et al (2011) Integrative genomics identifies MCU as an essential component of the mitochondrial calcium uniporter. Nature **476:** 341–345

Behera S, Kudla J (2013) High-resolution imaging of cytoplasmic Ca^{2+} dynamics in Arabidopsis roots. Cold Spring Harb Protoc **2013:** 669–672

Bick AG, Calvo SE, Mootha VK (2012) Evolutionary diversity of the mitochondrial calcium uniporter. Science **336:** 886

Braun CJ, Lachnit C, Becker P, Henkes LM, Arrigoni C, Kast SM, Moroni A, Thiel G, Schroeder I (2014) Viral potassium channels as a robust model system for studies of membrane-protein interaction. Biochim Biophys Acta **1838:** 1096–1103

Braun HP, Binder S, Brennicke A, Eubel H, Fernie AR, Finkemeier I, Klodmann J, König AC, Kühn K, Meyer E, et al (2014) The life of plant mitochondrial complex I. Mitochondrion **19:** 295–313

Carnieri EG, Martins IS, Vercesi AE (1987) The mechanism and biological role of calcium transport by plant mitochondria. Braz J Med Biol Res **20:** 635–638

Carraretto L, Formentin E, Teardo E, Checchetto V, Tomizioli M, Morosinotto T, Giacometti GM, Finazzi G, Szabó I (2013) A thylakoid-located two-pore K^+ channel controls photosynthetic light utilization in plants. Science **342:** 114–118

Carraretto L, Teardo E, Checchetto V, Finazzi G, Uozumi N, Szabò I (2016) Ion channels in plant bioenergetic organelles chloroplast and mitochondria: from molecular identification to function. Mol Plant **9:** 371–395

Chaudhuri D, Sancak Y, Mootha VK, Clapham DE (2013) MCU encodes the pore conducting mitochondrial calcium currents. eLife **2:** e00704

Curtis MD, Grossniklaus U (2003) A Gateway cloning vector set for high-throughput functional analysis of genes in planta. Plant Physiol **133:** 462–469

de Longevialle AF, Meyer EH, Andrés C, Taylor NL, Lurin C, Millar AH, Small ID (2007) The pentatricopeptide repeat gene *OTP43* is required for *trans*-splicing of the mitochondrial *nad1* intron 1 in *Arabidopsis thaliana*. Plant Cell **19:** 3256–3265

De Marchi U, Checchetto V, Zanetti M, Teardo E, Soccio M, Formentin E, Giacometti GM, Pastore D, Zoratti M, Szabò I (2010) ATP-sensitive cation-channel in wheat (*Triticum durum* Desf.): identification and characterization of a plant mitochondrial channel by patch-clamp. Cell Physiol Biochem **26:** 975–982

De Stefani D, Patron M, Rizzuto R (2015) Structure and function of the mitochondrial calcium uniporter complex. Biochim Biophys Acta **1853:** 2006–2011

De Stefani D, Raffaello A, Teardo E, Szabò I, Rizzuto R (2011) A forty-kilodalton protein of the inner membrane is the mitochondrial calcium uniporter. Nature **476:** 336–340

Dello Ioio R, Nakamura K, Moubayidin L, Perilli S, Taniguchi M, Morita MT, Aoyama T, Costantino P, Sabatini S (2008) A genetic framework for the control of cell division and differentiation in the root meristem. Science **322:** 1380–1384

Deniaud A, Liguori L, Blesneac I, Lenormand JL, Pebay-Peyroula E (2010) Crystallization of the membrane protein hVDAC1 produced in cell-free system. Biochim Biophys Acta **1798:** 1540–1546

Dieter P, Marmé D (1980) Ca^{2+} transport in mitochondrial and microsomal fractions from higher plants. Planta **150:** 1–8

Dodd AN, Kudla J, Sanders D (2010) The language of calcium signaling. Annu Rev Plant Biol **61:** 593–620

Fester T, Hause G (2005) Accumulation of reactive oxygen species in arbuscular mycorrhizal roots. Mycorrhiza **15:** 373–379

Fricker MD (2016) Quantitative redox imaging software. Antioxid Redox Signal **24:** 752–762

Foreman J, Demidchik V, Bothwell JH, Mylona P, Miedema H, Torres MA, Linstead P, Costa S, Brownlee C, Jones JD, Davies JM, Dolan L (2003) Reactive oxygen species produced by NADPH oxidase regulate plant cell growth. Nature **422:** 442–446

Foskett JK, Philipson B (2015) The mitochondrial Ca^{2+} uniporter complex. J Mol Cell Cardiol **78:** 3–8

Hanson JB, Malhotra SS, Stoner CD (1965) Action of calcium on corn mitochondria. Plant Physiol **40:** 1033–1040

Herdean A, Teardo E, Nilsson AK, Pfeil BE, Johansson ON, Ünnep R, Nagy G, Zsiros O, Dana S, Solymosi K, et al (2016) A voltage-dependent

chloride channel fine-tunes photosynthesis in plants. Nat Commun **7:** 11654

Hess P, Tsien RW (1984) Mechanism of ion permeation through calcium channels. Nature **309:** 453–456

Hille B (1978) Ionic channels in excitable membranes. Current problems and biophysical approaches. Biophys J **22:** 283–294

Huang G, Vercesi AE, Docampo R (2013) Essential regulation of cell bioenergetics in *Trypanosoma brucei* by the mitochondrial calcium uniporter. Nat Commun **4:** 2865

Huang S, Millar AH (2013) Succinate dehydrogenase: the complex roles of a simple enzyme. Curr Opin Plant Biol **16:** 344–349

Huang S, Van Aken O, Schwarzländer M, Belt K, Millar AH (2016) Roles of mitochondrial reactive oxygen species in cellular signalling and stress response in plants. Plant Physiol **171:** 1551–1559

Huelsenbeck JP, Ronquist F (2001) MRBAYES: Bayesian inference of phylogenetic trees. Bioinformatics **17:** 754–755

Jardim-Messeder D, Caverzan A, Rauber R, de Souza Ferreira E, Margis-Pinheiro M, Galina A (2015) Succinate dehydrogenase (mitochondrial complex II) is a source of reactive oxygen species in plants and regulates development and stress responses. New Phytol **208:** 776–789

Jia L (2011) Is reactive oxygen species (ROS) the underlying factor for inhibited root growth in Osspr1? Plant Signal Behav **6:** 1024–1025

Karniely S, Pines O (2005) Single translation–dual destination: mechanisms of dual protein targeting in eukaryotes. EMBO Rep **6:** 420–425

Kirichok Y, Krapivinsky G, Clapham DE (2004) The mitochondrial calcium uniporter is a highly selective ion channel. Nature **427:** 360–364

Klodmann J, Senkler M, Rode C, Braun HP (2011) Defining the protein complex proteome of plant mitochondria. Plant Physiol **157:** 587–598

Kmiecik P, Leonardelli M, Teige M (2016) Novel connections in plant organellar signalling link different stress responses and signalling pathways. J Exp Bot **67:** 3793–3807

Kovács-Bogdán E, Sancak Y, Kamer KJ, Plovanich M, Jambhekar A, Huber RJ, Myre MA, Blower MD, Mootha VK (2014) Reconstitution of the mitochondrial calcium uniporter in yeast. Proc Natl Acad Sci USA **111:** 8985–8990

Larosa V, Coosemans N, Motte P, Bonnefoy N, Remacle C (2012) Reconstruction of a human mitochondrial complex I mutation in the unicellular green alga Chlamydomonas. Plant J **70:** 759–768

Lee CP, Eubel H, O'Toole N, Millar AH (2008) Heterogeneity of the mitochondrial proteome for photosynthetic and non-photosynthetic Arabidopsis metabolism. Mol Cell Proteomics **7:** 1297–1316

Lepple-Wienhues A, Cahalan MD (1996) Conductance and permeation of monovalent cations through depletion-activated Ca^{2+} channels (ICRAC) in Jurkat T cells. Biophys J **71:** 787–794

Livak KJ, Schmittgen TD (2001) Analysis of relative gene expression data using real-time quantitative PCR and the 2(-Delta Delta C(T)) method. Methods **25:** 402–408

Logan CV, Szabadkai G, Sharpe JA, Parry DA, Torelli S, Childs AM, Kriek M, Phadke R, Johnson CA, Roberts NY, et al; UK10K Consortium (2014) Loss-of-function mutations in MICU1 cause a brain and muscle disorder linked to primary alterations in mitochondrial calcium signaling. Nat Genet **46:** 188–193

Logan DC, Knight MR (2003) Mitochondrial and cytosolic calcium dynamics are differentially regulated in plants. Plant Physiol **133:** 21–24

Logan DC, Leaver CJ (2000) Mitochondria-targeted GFP highlights the heterogeneity of mitochondrial shape, size and movement within living plant cells. J Exp Bot **51:** 865–871

Loro G, Drago I, Pozzan T, Schiavo FL, Zottini M, Costa A (2012) Targeting of Cameleons to various subcellular compartments reveals a strict cytoplasmic/mitochondrial Ca^{2+} handling relationship in plant cells. Plant J **71:** 1–13

Love J, Dodd AN, Webb AA (2004) Circadian and diurnal calcium oscillations encode photoperiodic information in Arabidopsis. Plant Cell **16:** 956–966

Mallilankaraman K, Cárdenas C, Doonan PJ, Chandramoorthy HC, Irrinki KM, Golenár T, Csordás G, Madireddi P, Yang J, Müller M, et al (2012) MCUR1 is an essential component of mitochondrial Ca^{2+} uptake that regulates cellular metabolism. Nat Cell Biol **14:** 1336–1343

Mammucari C, Gherardi G, Zamparo I, Raffaello A, Boncompagni S, Chemello F, Cagnin S, Braga A, Zanin S, Pallafacchina G, et al (2015) The mitochondrial calcium uniporter controls skeletal muscle trophism in vivo. Cell Reports **10:** 1269–1279

Lee Y, Min CK, Kim TG, Song HK, Lim Y, Kim D, Shin K, Kang M, Kang JY, Youn HS, et al (2015) Structure and function of the N-terminal domain of the human mitochondrial calcium uniporter. EMBO Rep **16:** 1318–1333

Martins IS, Vercesi AE (1985) Some characteristics of Ca^{2+} transport in plant mitochondria. Biochem Biophys Res Commun **129:** 943–948

McAinsh MR, Pittman JK (2009) Shaping the calcium signature. New Phytol **181:** 275–294

Meng Q, Chen Y, Zhang M, Chen Y, Yuan J, Murray SC (2015) Molecular characterization and phylogenetic analysis of ZmMCUs in maize. Biologia **70:** 599–605

Millar AH, Eubel H, Jänsch L, Kruft V, Heazlewood JL, Braun HP (2004) Mitochondrial cytochrome *c* oxidase and succinate dehydrogenase complexes contain plant specific subunits. Plant Mol Biol **56:** 77–90

Murphy E, Pan X, Nguyen T, Liu J, Holmström KM, Finkel T (2014) Unresolved questions from the analysis of mice lacking MCU expression. Biochem Biophys Res Commun **449:** 384–385

Nomura H, Shiina T (2014) Calcium signaling in plant endosymbiotic organelles: mechanism and role in physiology. Mol Plant **7:** 1094–1104

Oxenoid K, Dong Y, Cao C, Cui T, Sancak Y, Markhard AL, Grabarek Z, Kong L, Liu Z, Ouyang B, et al (2016) Architecture of the mitochondrial calcium uniporter. Nature **533:** 269–273

Pan X, Liu J, Nguyen T, Liu C, Sun J, Teng Y, Fergusson MM, Rovira II, Allen M, Springer DA, et al (2013) The physiological role of mitochondrial calcium revealed by mice lacking the mitochondrial calcium uniporter. Nat Cell Biol **15:** 1464–1472

Patron M, Checchetto V, Raffaello A, Teardo E, Vecellio Reane D, Mantoan M, Granatiero V, Szabò I, De Stefani D, Rizzuto R (2014) MICU1 and MICU2 finely tune the mitochondrial Ca^{2+} uniporter by exerting opposite effects on MCU activity. Mol Cell **53:** 726–737

Paupe V, Prudent J, Dassa EP, Rendon OZ, Shoubridge EA (2015) CCDC90A (MCUR1) is a cytochrome *c* oxidase assembly factor and not a regulator of the mitochondrial calcium uniporter. Cell Metab **21:** 109–116

Perocchi F, Gohil VM, Girgis HS, Bao XR, McCombs JE, Palmer AE, Mootha VK (2010) MICU1 encodes a mitochondrial EF hand protein required for Ca^{2+} uptake. Nature **467:** 291–296

Petrungaro C, Zimmermann KM, Küttner V, Fischer M, Dengjel J, Bogeski I, Riemer J (2015) The Ca^{2+}-dependent release of the Mia40-induced MICU1-MICU2 dimer from MCU regulates mitochondrial Ca^{2+} uptake. Cell Metab **22:** 721–733

Plovanich M, Bogorad RL, Sancak Y, Kamer KJ, Strittmatter L, Li AA, Girgis HS, Kuchimanchi S, De Groot J, Speciner L, et al (2013) MICU2, a paralog of MICU1, resides within the mitochondrial uniporter complex to regulate calcium handling. PLoS One **8:** e55785

Prudent J, Popgeorgiev N, Bonneau B, Thibaut J, Gadet R, Lopez J, Gonzalo P, Rimokh R, Manon S, Houart C, et al (2013) Bcl-wav and the mitochondrial calcium uniporter drive gastrula morphogenesis in zebrafish. Nat Commun **4:** 2330

Pu X, Lv X, Tan T, Fu F, Qin G, Lin H (2015) Roles of mitochondrial energy dissipation systems in plant development and acclimation to stress. Ann Bot (Lond) **116:** 583–600

Quan X, Nguyen TT, Choi SK, Xu S, Das R, Cha SK, Kim N, Han J, Wiederkehr A, Wollheim CB, et al (2015) Essential role of mitochondrial Ca^{2+} uniporter in the generation of mitochondrial pH gradient and metabolism-secretion coupling in insulin-releasing cells. J Biol Chem **290:** 4086–4096

Raffaello A, De Stefani D, Sabbadin D, Teardo E, Merli G, Picard A, Checchetto V, Moro S, Szabò I, Rizzuto R (2013) The mitochondrial calcium uniporter is a multimer that can include a dominant-negative pore-forming subunit. EMBO J **32:** 2362–2376

Rasmussen TP, Wu Y, Joiner ML, Koval OM, Wilson NR, Luczak ED, Wang Q, Chen B, Gao Z, Zhu Z, et al (2015) Inhibition of MCU forces extramitochondrial adaptations governing physiological and pathological stress responses in heart. Proc Natl Acad Sci USA **112:** 9129–9134

Rizzuto R, De Stefani D, Raffaello A, Mammucari C (2012) Mitochondria as sensors and regulators of calcium signalling. Nat Rev Mol Cell Biol **13:** 566–578

Sancak Y, Markhard AL, Kitami T, Kovács-Bogdán E, Kamer KJ, Udeshi ND, Carr SA, Chaudhuri D, Clapham DE, Li AA, et al (2013) EMRE is an essential component of the mitochondrial calcium uniporter complex. Science **342:** 1379–1382

Schwacke R, Schneider A, van der Graaff E, Fischer K, Catoni E, Desimone M, Frommer WB, Flügge UI, Kunze R (2003) ARAMEMNON, a novel

database for Arabidopsis integral membrane proteins. Plant Physiol **131:** 16–26

Senkler J, Senkler M, Eubel H, Hildebrandt T, Lengwenus C, Schertl P, Schwarzländer M, Wagner S, Wittig I, Braun HP (2016) The mitochondrial complexome of *Arabidopsis thaliana*. Plant J, doi/10.1111/tpj.13448

Silva MA, Carnieri EG, Vercesi AE (1992) Calcium transport by corn mitochondria: evaluation of the role of phosphate. Plant Physiol **98:** 452–457

Stael S, Wurzinger B, Mair A, Mehlmer N, Vothknecht UC, Teige M (2012) Plant organellar calcium signalling: an emerging field. J Exp Bot **63:** 1525–1542

Sweetlove LJ, Taylor NL, Leaver CJ (2007) Isolation of intact, functional mitochondria from the model plant *Arabidopsis thaliana*. Methods Mol Biol **372:** 125–136

Szabò I, Zoratti M (2014) Mitochondrial channels: ion fluxes and more. Physiol Rev **94:** 519–608

Talavera K, Nilius B (2006) Biophysics and structure-function relationship of T-type Ca^{2+} channels. Cell Calcium **40:** 97–114

Teardo E, Carraretto L, De Bortoli S, Costa A, Behera S, Wagner R, Lo Schiavo F, Formentin E, Szabò I (2015) Alternative splicing-mediated targeting of the Arabidopsis GLUTAMATE RECEPTOR3.5 to mitochondria affects organelle morphology. Plant Physiol **167:** 216–227

Teardo E, Formentin E, Segalla A, Giacometti GM, Marin O, Zanetti M, Lo Schiavo F, Zoratti M, Szabò I (2011) Dual localization of plant glutamate receptor AtGLR3.4 to plastids and plasmamembrane. Biochim Biophys Acta **1807:** 359–367

Tsukagoshi H (2016) Control of root growth and development by reactive oxygen species. Curr Opin Plant Biol **29:** 57–63

Tsukagoshi H, Busch W, Benfey PN (2010) Transcriptional regulation of ROS controls transition from proliferation to differentiation in the root. Cell **143:** 606–616

Vais H, Mallilankaraman K, Mak DO, Hoff H, Payne R, Tanis JE, Foskett JK (2016) EMRE is a matrix Ca^{2+} sensor that governs gatekeeping of the mitochondrial Ca^{2+} uniporter. Cell Reports **14:** 403–410

Vais H, Tanis JE, Müller M, Payne R, Mallilankaraman K, Foskett JK (2015) MCUR1, CCDC90A, is a regulator of the mitochondrial calcium uniporter. Cell Metab **22:** 533–535

van den Berg C, Willemsen V, Hendriks G, Weisbeek P, Scheres B (1997) Short-range control of cell differentiation in the Arabidopsis root meristem. Nature **390:** 287–289

Vecellio Reane D, Vallese F, Checchetto V, Acquasaliente L, Butera G, De Filippis V, Szabò I, Zanotti G, Rizzuto R, Raffaello A (2016) A MICU1 splice variant confers high sensitivity to the mitochondrial Ca^{2+} uptake machinery of skeletal muscle. Mol Cell **64:** 760–773

Virolainen E, Blokhina O, Fagerstedt K (2002) Ca^{2+}-induced high amplitude swelling and cytochrome *c* release from wheat (*Triticum aestivum* L.) mitochondria under anoxic stress. Ann Bot (Lond) **90:** 509–516

Wagner S, Behera S, De Bortoli S, Logan DC, Fuchs P, Carraretto L, Teardo E, Cendron L, Nietzel T, Füßl M, et al (2015) The EF-hand Ca^{2+} binding protein MICU choreographs mitochondrial Ca^{2+} dynamics in Arabidopsis. Plant Cell **27:** 3190–3212

Wagner S, De Bortoli S, Schwarzländer M, Szabò I (2016) Regulation of mitochondrial calcium in plants versus animals. J Exp Bot **67:** 3809–3829

Weber AP, Linka N (2011) Connecting the plastid: transporters of the plastid envelope and their role in linking plastidial with cytosolic metabolism. Annu Rev Plant Biol **62:** 53–77

Zimmermann P, Hirsch-Hoffmann M, Hennig L, Gruissem W (2004) GENEVESTIGATOR. Arabidopsis microarray database and analysis toolbox. Plant Physiol **136:** 2621–2632

Zottini M, Zannoni D (1993) The use of Fura-2 fluorescence to monitor the movement of free calcium ions into the matrix of plant mitochondria (*Pisum sativum* and *Helianthus tuberosus*). Plant Physiol **102:** 573–578